

Denoising Hyperbolic-Valued Data by Relaxed Regularizations

R. Beinert and J. Bresch

Technische Universität Berlin, Institute of Mathematics, Straße des 17. Juni 136,
10623 Berlin, Germany {beinert, bresch}@math.tu-berlin.de

Abstract. We introduce a novel relaxation strategy for denoising hyperbolic-valued data. The main challenge is here the non-convexity of the hyperbolic sheet. Instead of considering the denoising problem directly on the hyperbolic space, we exploit the Euclidean embedding and encode the hyperbolic sheet using a novel matrix representation. For denoising, we employ the Euclidean Tikhonov and total variation (TV) model, where we incorporate our matrix representation. The major contribution is then a convex relaxation of the variational ansätze allowing the utilization of well-established convex optimization procedures like the alternating directions method of multipliers (ADMM). The resulting denoisers are applied to a real-world Gaussian image processing task, where we simultaneously restore the pixelwise mean and standard deviation of a retina scan series.

Keywords: Hyperbolic-valued data · Signal and image processing · TV denoising · Tikhonov denoising · Convex relaxation methods.

1 Introduction

The geometry of hyperbolic spaces finds applications across diverse research fields spanning from theoretical studies in mathematics and physics to practical implementations in machine learning, network analysis, and computer vision. One of the most famous example is the specific relativity theory, where hyperbolic spaces and their geometry are often used to model the spacetime [24]. Moreover, hyperbolic spaces are particularly well-suited for capturing hierarchical structures, such as those found in social and biological networks as well as in the topology of the internet [7, 18]. In order to analyse hierarchical or tree-like data, the hyperbolic geometry has been incorporated into machine learning architectures leading to so-called hyperbolic neural networks [13, 22], which, for instance, play a major role in hierarchical clustering [21, 23]. From the view point of image analysis, hyperbolic spaces become interesting due to their utilization in image segmentation [2], image denoising [6], and morphological image processing [1]. Hyperbolic-valued images, for instance, occur in probabilistic image analysis [1, 6], where each pixel is described by a Gaussian distribution, and as structure tensor in edge and texture processing [9].

Mathematically, the *hyperbolic space* \mathbb{H}_d is the unique, simply connected, d -dimensional Riemannian manifold with constant curvature of -1 , see [15, 17]. The hyperbolic spaces possess several different embeddings [20]. Throughout this paper, we rely on the Euclidean one:

$$\mathbb{H}_d := \{\mathbf{x} \in \mathbb{R}^{d+1} : \eta(\mathbf{x}, \mathbf{x}) = -1 \text{ and } x_{d+1} > 0\}$$

where $\eta: \mathbb{H}_d \times \mathbb{H}_d \rightarrow \mathbb{R}, (\mathbf{x}, \mathbf{y}) \mapsto \sum_{i=1}^d x_i y_i - x_{d+1} y_{d+1}$ is the *Minkowski bilinearform* defining the *hyperbolic distance* $\text{dist}_{\mathbb{H}_d}(\mathbf{x}, \mathbf{y}) := \text{arcosh}(-\eta(\mathbf{x}, \mathbf{y}))$. Note that the Euclidean embedding of the hyperbolic space \mathbb{H}_d , which is sometimes called the *hyperbolic sheet*, is contained in the $(d+1)$ -dimensional, affine halfspace $\mathbb{A}_{d+1} := \mathbb{R}^d \times \mathbb{R}_{\geq 1}$, i.e. $\mathbb{H}_d \subset \mathbb{A}_{d+1}$.

In this paper, we approach the problem of hyperbolic image denoising. Here, the main issue comes from the non-convexity of the hyperbolic sheet. This is why hyperbolic image denoising becomes highly demanding from a numerical point of view. For instance, hyperbolic images can be denoised using total variation (TV) models based on the hyperbolic distance and applying a manifold version of the Douglas–Rachford algorithm [6]. The major contribution of this paper is that, instead of minimizing a variational denoising model directly on the hyperbolic sheet \mathbb{H}_d , we exploit the Euclidean embedding and propose a novel convex relaxation that allows the application of well-established convex optimization methods on \mathbb{R}^{d+1} . The paper is organized as follows: In § 2, we introduce (Euclidean) TV- and Tikhonov-like regularization models and convex relaxations that encode the hyperbolic sheet using positive semi-definite matrices in the spirit of [4, 5, 12]. In § 3, we use the alternating directions method of multipliers (ADMM) [14] to derive an actual denoising algorithm. Finally, in § 4, we apply the proposed method to denoising problems from Gaussian image processing.

2 Denoising of Hyperbolic-Valued Data

The aim of this paper is to denoise hyperbolic-valued data on a connected, undirected graph $G = (V, E)$, where $V := \{1, \dots, N\}$ denotes the set of N vertices and $E \subseteq \{(n, m) \in V \times V : n < m\}$ the set of $M := |E|$ edges. We are now interested in the restoration of hyperbolic-valued data $\mathbf{x} := (\mathbf{x}_n)_{n \in V} \in \mathbb{H}_d^N$ from noisy measurements $\mathbf{y} := (\mathbf{y}_n)_{n \in V}$ in \mathbb{H}_d^N or $(\mathbb{R}^{d+1})^N$. For applications in signal and image processing, G corresponds to the line or grid graph.

2.1 Tikhonov-like Regularization

For denoising relatively smooth hyperbolic data, we consider the variational Tikhonov-like denoising model:

$$\arg \min_{\mathbf{x} \in \mathbb{H}_d^N} \frac{1}{2} \sum_{n \in V} \|\mathbf{x}_n - \mathbf{y}_n\|_2^2 + \frac{\lambda}{2} \sum_{(n, m) \in E} \|\mathbf{x}_n - \mathbf{x}_m\|_2^2, \quad (1)$$

where $\|\cdot\|_2$ denotes the Euclidean norm, and $\lambda > 0$ the regularization parameter. Note that the model (1) is non-convex due to the minimization of the hyperbolic sheet. In order to convexify (1), we adapt the strategies in [5, 12], where the Tikhonov denoising for the hypersphere and $\text{SO}(3)$ is considered. For this, we introduce the auxiliary variables $\mathbf{f} \in \mathbb{R}^M$ and $\mathbf{v} \in \mathbb{R}^N$ and the linear objective

$$\mathcal{J}(\mathbf{x}, \mathbf{f}, \mathbf{v}) := \frac{1}{2} \sum_{n \in V} (\mathbf{v}_n - 2\langle \mathbf{x}_n, \mathbf{y}_n \rangle) + \frac{\lambda}{2} \sum_{(n,m) \in E} (\mathbf{v}_n + \mathbf{v}_m - 2\mathbf{f}_{(n,m)}) \quad (2)$$

with the Euclidean inner product $\langle \cdot, \cdot \rangle$. Therewith, (1) becomes equivalent to

$$\arg \min_{\mathbf{x} \in \mathbb{H}_d^N} \mathcal{J}(\mathbf{x}, \mathbf{f}, \mathbf{v}) \quad \text{s.t.} \quad \left\{ \begin{array}{ll} \mathbf{v}_n = \|\mathbf{x}_n\|_2^2 & \forall n \in V \\ \mathbf{f}_{(n,m)} = \langle \mathbf{x}_n, \mathbf{x}_m \rangle & \forall (n,m) \in E \end{array} \right\}. \quad (3)$$

For any $\boldsymbol{\xi} \in \mathbb{R}^{d+1}$, we define $\tilde{\boldsymbol{\xi}} := (\xi_1, \dots, \xi_d, -\xi_{d+1})^*$. Further, we denote the $(d+1) \times (d+1)$ identity by \mathbf{I}_{d+1} . To encode the minimization over the hyperbolic sheet, we introduce—based on the additional variables $\boldsymbol{\ell} \in \mathbb{R}^M$ —the series of matrices

$$\mathbf{Q}_{(n,m)} := \begin{bmatrix} \mathbf{I}_{d+1} & \mathbf{x}_n & \tilde{\mathbf{x}}_n & \mathbf{x}_m & \tilde{\mathbf{x}}_m \\ \mathbf{x}_n^* & \mathbf{v}_n & -1 & \mathbf{f}_{(n,m)} & \boldsymbol{\ell}_{(n,m)} \\ \tilde{\mathbf{x}}_n^* & -1 & \mathbf{v}_n & \boldsymbol{\ell}_{(n,m)} & \mathbf{f}_{(n,m)} \\ \mathbf{x}_m^* & \mathbf{f}_{(n,m)} & \boldsymbol{\ell}_{(n,m)} & \mathbf{v}_m & -1 \\ \tilde{\mathbf{x}}_m^* & \boldsymbol{\ell}_{(n,m)} & \mathbf{f}_{(n,m)} & -1 & \mathbf{v}_m \end{bmatrix}.$$

Proposition 1. *Let $\mathbf{x}_n, \mathbf{x}_m \in \mathbb{A}_{d+1}$. Then $\mathbf{x}_n, \mathbf{x}_m \in \mathbb{H}_d$, $\mathbf{v}_n = \|\mathbf{x}_n\|_2^2$, $\mathbf{v}_m = \|\mathbf{x}_m\|_2^2$, $\boldsymbol{\ell}_{(n,m)} = \eta(\mathbf{x}_n, \mathbf{x}_m)$, and $\mathbf{f}_{(n,m)} = \langle \mathbf{x}_n, \mathbf{x}_m \rangle$ if and only if $\mathbf{Q}_{(n,m)} \succeq \mathbf{0}$ and $\text{rank}(\mathbf{Q}_{(n,m)}) = d+1$.*

Proof. Because of the identity in the upper left, $\mathbf{Q}_{(n,m)}$ has at least rank $d+1$. Now, the last four rows can be represented by the first $d+1$ rows if and only if $\mathbf{v}_n = \|\mathbf{x}_n\|_2^2$, $\mathbf{v}_m = \|\mathbf{x}_m\|_2^2$, $\boldsymbol{\ell}_{(n,m)} = \eta(\mathbf{x}_n, \mathbf{x}_m)$, $\mathbf{f}_{(n,m)} = \langle \mathbf{x}_n, \mathbf{x}_m \rangle$ as well as $\eta(\mathbf{x}_n, \mathbf{x}_n) = -1$ and $\eta(\mathbf{x}_m, \mathbf{x}_m) = -1$, i.e. $\mathbf{x}_n, \mathbf{x}_m \in \mathbb{H}_d$. Applying Schur's theorem [16], we have $\mathbf{Q}_{(n,m)} \succeq \mathbf{0}$ if and only if the Schur complement

$$\mathbf{Q}_{(n,m)}/\mathbf{I}_{d+1} = \begin{bmatrix} \mathbf{v}_n - \|\mathbf{x}_n\|_2^2 & -1 - \eta(\mathbf{x}_n, \mathbf{x}_n) & \mathbf{f}_{(n,m)} - \langle \mathbf{x}_n, \mathbf{x}_m \rangle & \boldsymbol{\ell}_{(n,m)} - \eta(\mathbf{x}_n, \mathbf{x}_m) \\ -1 - \eta(\mathbf{x}_n, \mathbf{x}_n) & \mathbf{v}_n - \|\mathbf{x}_n\|_2^2 & \boldsymbol{\ell}_{(n,m)} - \eta(\mathbf{x}_n, \mathbf{x}_m) & \mathbf{f}_{(n,m)} - \langle \mathbf{x}_n, \mathbf{x}_m \rangle \\ \mathbf{f}_{(n,m)} - \langle \mathbf{x}_n, \mathbf{x}_m \rangle & \boldsymbol{\ell}_{(n,m)} - \eta(\mathbf{x}_n, \mathbf{x}_m) & \mathbf{v}_m - \|\mathbf{x}_m\|_2^2 & -1 - \eta(\mathbf{x}_m, \mathbf{x}_m) \\ \boldsymbol{\ell}_{(n,m)} - \eta(\mathbf{x}_n, \mathbf{x}_m) & \mathbf{f}_{(n,m)} - \langle \mathbf{x}_n, \mathbf{x}_m \rangle & -1 - \eta(\mathbf{x}_m, \mathbf{x}_m) & \mathbf{v}_m - \|\mathbf{x}_m\|_2^2 \end{bmatrix}$$

is positive semi-definite. Under the given assumptions, $\mathbf{Q}_{(n,m)}/\mathbf{I}_{d+1}$ becomes zero and hence positive semi-definite. \square

In light of Prop. 1, the Tikhonov-like denoising model (3) is equivalent to

$$\arg \min_{\substack{\mathbf{x} \in \mathbb{A}_{d+1}^N, \boldsymbol{\ell} \in \mathbb{R}^M, \\ \mathbf{f} \in \mathbb{R}^M, \mathbf{v} \in \mathbb{R}^N}} \mathcal{J}(\mathbf{x}, \mathbf{f}, \mathbf{v}) \quad \text{s.t.} \quad \left\{ \begin{array}{l} \mathbf{Q}_{(n,m)} \succeq \mathbf{0} \\ \text{rank}(\mathbf{Q}_{(n,m)}) = d+1 \end{array} \right\} \quad \forall (n,m) \in E. \quad (4)$$

In the manner of [5], we convexify (4) by neglecting the non-convex rank-constraints. Thus, we propose to solve the convex *relaxed Tikhonov denoising model*:

$$\arg \min_{\substack{\mathbf{x} \in \mathbb{A}_{d+1}^N, \boldsymbol{\ell} \in \mathbb{R}^M, \\ \mathbf{f} \in \mathbb{R}^M, \mathbf{v} \in \mathbb{R}^N}} \mathcal{J}(\mathbf{x}, \mathbf{f}, \mathbf{v}) \quad \text{s.t.} \quad \mathbf{Q}_{(n,m)} \succeq \mathbf{0} \quad \forall (n,m) \in E. \quad (5)$$

2.2 TV Regularization

For denoising cartoon-like data, the Tikhonov denoising model in § 2.1 is not suitable. Instead, we consider the variational TV denoising model:

$$\arg \min_{\mathbf{x} \in \mathbb{H}_d^N} \frac{1}{2} \sum_{n \in V} \|\mathbf{x}_n - \mathbf{y}_n\|_2^2 + \mu \text{TV}(\mathbf{x}), \quad \text{where} \quad \text{TV}(\mathbf{x}) := \sum_{(n,m) \in E} \|\mathbf{x}_n - \mathbf{x}_m\|_1 \quad (6)$$

and $\|\cdot\|_1$ denotes the Manhattan norm, and $\mu > 0$ is the regularization parameter. In the manner of [4], where the TV denoising on the hypersphere and $\text{SO}(3)$ is considered, we introduce the auxiliary parameter $\mathbf{v} \in \mathbb{R}^N$ and the (non-linear) objective

$$\mathcal{K}(\mathbf{x}, \mathbf{v}) := \frac{1}{2} \sum_{n \in V} (\mathbf{v}_n - 2\langle \mathbf{x}_n, \mathbf{y}_n \rangle) + \mu \text{TV}(\mathbf{x}).$$

Hence, (6) becomes equivalent to

$$\arg \min_{\mathbf{x} \in \mathbb{H}_d^N} \mathcal{K}(\mathbf{x}, \mathbf{v}) \quad \text{s.t.} \quad \mathbf{v}_n = \|\mathbf{x}_n\|_2^2 \quad \forall n \in V. \quad (7)$$

Applying Prop. 1, we may rewrite (7) as

$$\arg \min_{\substack{\mathbf{x} \in \mathbb{A}_{d+1}^N, \ell \in \mathbb{R}^M \\ \mathbf{f} \in \mathbb{R}^M, \mathbf{v} \in \mathbb{R}^N}} \mathcal{K}(\mathbf{x}, \mathbf{v}) \quad \text{s.t.} \quad \left\{ \begin{array}{l} \mathbf{Q}_{(n,m)} \succeq 0 \\ \text{rank}(\mathbf{Q}_{(n,m)}) = d+1 \end{array} \right\} \quad \forall (n,m) \in E. \quad (8)$$

Different from § 2.1, where \mathbf{f} is essential to linearize the objective, and where $\mathbf{Q}_{(n,m)}$ encodes $\mathbf{f}_{(n,m)} = \langle \mathbf{x}_n, \mathbf{x}_m \rangle$, the auxiliary variables \mathbf{f} and ℓ here seem to be superfluous. We derive an alternative encoding of the hyperbolic sheet.

Proposition 2. *Let $\mathbf{x}_n \in \mathbb{A}_{d+1}$. Then $\mathbf{x}_n \in \mathbb{H}_d$ and $\mathbf{v}_n = \|\mathbf{x}_n\|_2^2$ if and only if*

$$\mathbf{V}_n := \begin{bmatrix} \mathbf{I}_{d+1} & \mathbf{x}_n & \tilde{\mathbf{x}}_n \\ \mathbf{x}_n^* & \mathbf{v}_n & -1 \\ \tilde{\mathbf{x}}_n^* & -1 & \mathbf{v}_n \end{bmatrix} \succeq 0 \quad \text{and} \quad \text{rank}(\mathbf{V}_n) = d+1.$$

The statement can be established in analogy to Prop. 1 using Schur's theorem. On the basis of Prop. 2, the TV denoising model (7) is also equivalent to

$$\arg \min_{\mathbf{x} \in \mathbb{A}_{d+1}^N, \mathbf{v} \in \mathbb{R}^N} \mathcal{K}(\mathbf{x}, \mathbf{v}) \quad \text{s.t.} \quad \left\{ \begin{array}{l} \mathbf{V}_{(n)} \succeq 0 \\ \text{rank}(\mathbf{V}_{(n)}) = d+1 \end{array} \right\} \quad \text{for all } n \in V.$$

Neglecting the rank constraint, we propose to solve the convex *relaxed TV denoising model*:

$$\arg \min_{\mathbf{x} \in \mathbb{A}_{d+1}^N, \mathbf{v} \in \mathbb{R}^N} \mathcal{K}(\mathbf{x}, \mathbf{v}) \quad \text{s.t.} \quad \mathbf{V}_n \succeq 0 \quad \forall n \in V. \quad (9)$$

Notice that the relaxed version of (8)—without the rank constraint—and the proposed model (9) are equivalent: if $(\hat{\mathbf{x}}, \hat{\ell}, \hat{\mathbf{f}}, \hat{\mathbf{v}})$ is a solution of the relaxed version of (8), then $(\hat{\mathbf{x}}, \hat{\mathbf{v}})$ is a solution of (9); if $(\hat{\mathbf{x}}, \hat{\mathbf{v}})$ is a solution of (9), then $(\hat{\mathbf{x}}, (\eta(\hat{\mathbf{x}}_n, \hat{\mathbf{x}}_m))_{(n,m) \in E}, (\langle \hat{\mathbf{x}}_n, \hat{\mathbf{x}}_m \rangle)_{(n,m) \in E}, \hat{\mathbf{v}})$ is a solution of the relaxed version of (8). The positive semi-definiteness can be transferred between $\mathbf{Q}_{(n,m)}$, \mathbf{V}_n , and \mathbf{V}_m utilizing Schur's theorem and Sylvester's criterion [16].

3 Denoising Models and Algorithms

In this section we solve both convex relaxed problems, defined in (5) and (9), employing the alternating directions methods of multipliers (ADMM) [14]. In general, ADMM allows to solve convex minimization problems of the form

$$\arg \min_{\mathbf{Y}, \mathbf{U}} \mathcal{F}(\mathbf{Y}) + \mathcal{G}(\mathbf{U}) \quad \text{s.t.} \quad \mathcal{L}(\mathbf{Y}) = \mathbf{U}, \quad (10)$$

where \mathcal{F} and \mathcal{G} are convex, and \mathcal{L} is linear, using the iteration:

$$\mathbf{Y}^{(k+1)} := \arg \min_{\mathbf{Y}} \mathcal{F}(\mathbf{Y}) + \frac{\rho}{2} \|\mathcal{L}(\mathbf{Y}) - \mathbf{U}^{(k)} + \mathbf{Z}^{(k)}\|^2, \quad (11a)$$

$$\mathbf{U}^{(k+1)} := \arg \min_{\mathbf{U}} \mathcal{G}(\mathbf{U}) + \frac{\rho}{2} \|\mathcal{L}(\mathbf{Y}^{(k+1)}) - \mathbf{U} + \mathbf{Z}^{(k)}\|^2, \quad (11b)$$

$$\mathbf{Z}^{(k+1)} := \mathbf{Z}^{(k)} + \mathcal{L}(\mathbf{Y}^{(k+1)}) - \mathbf{U}^{(k+1)}. \quad (11c)$$

3.1 Solving the Relaxed Tikhonov-like denoising model

To solve (5), we rely on the following splitting:

$$\arg \min_{\mathbf{x}, \boldsymbol{\ell}, \mathbf{f}, \mathbf{v}, \mathbf{U}} \mathcal{J}(\mathbf{x}, \mathbf{f}, \mathbf{v}) + \mathcal{I}(\mathbf{x}) + \mathcal{G}(\mathbf{U}) \quad \text{s.t.} \quad \mathcal{Q}(\mathbf{x}, \boldsymbol{\ell}, \mathbf{f}, \mathbf{v}) = \mathbf{U} \in \mathcal{S}_{d+5}^M, \quad (12)$$

where \mathcal{S}_{d+5} denotes the symmetric $(d+5) \times (d+5)$ matrices. Using the indicator function ι_{\bullet} , which is zero on the indicated set and $+\infty$ otherwise, we define

$$\mathcal{I}(\mathbf{x}) := \sum_{n \in V} \iota_{\mathbb{A}_{d+1}}(\mathbf{x}_n) \quad \text{and} \quad \mathcal{G}(\mathbf{U}) := \sum_{(n,m) \in E} \iota_{\mathcal{C}}(\mathbf{U}_{(n,m)}) \quad (13)$$

with $\mathbf{E} := \text{diag}(\mathbf{I}_{d+1}, \begin{bmatrix} 0 & -1 \\ -1 & 0 \end{bmatrix}, \begin{bmatrix} 0 & -1 \\ -1 & 0 \end{bmatrix})$ and $\mathcal{C} := \{\mathbf{A} \in \mathcal{S}_{d+5} : \mathbf{A} \succeq -\mathbf{E}\}$. Finally, the linear operator $\mathcal{Q} := (\mathcal{Q}_{(n,m)})_{(n,m) \in E}$ is defined as

$$\mathcal{Q}_{(n,m)}(\mathbf{x}, \boldsymbol{\ell}, \mathbf{f}, \mathbf{v}) := \mathbf{Q}_{(n,m)} - \mathbf{E}.$$

To apply (11), we define $\|\mathbf{U}\|^2 := \sum_{(n,m) \in E} \|\mathbf{U}_{(n,m)}\|_{\text{F}}^2$, where $\|\cdot\|_{\text{F}}$ denotes the Frobenius norm. Further, we require the adjoint of \mathcal{Q} . Based on the Kronecker delta $\delta_{i,j}$, the adjoint of \mathcal{Q} with respect to the argument \mathbf{x} is given by

$$((\mathcal{Q}_{\mathbf{x}}^*(\mathbf{U}))_n)_i = 2 \left[\sum_{(n,m) \in E} (\mathbf{U}_{(n,m)})_{i,d+2} + (-1)^{\delta_{i,d+1}} (\mathbf{U}_{(n,m)})_{i,d+3} \right] + 2 \left[\sum_{(m,n) \in E} (\mathbf{U}_{(m,n)})_{i,d+4} + (-1)^{\delta_{i,d+1}} (\mathbf{U}_{(m,n)})_{i,d+5} \right]$$

for $n \in V$ and $1 \leq i \leq d+1$; the adjoint with respect to $\boldsymbol{\ell}$ and \mathbf{f} are given by

$$(\mathcal{Q}_{\boldsymbol{\ell}}^*(\mathbf{U}))_{(n,m)} = 2 [(\mathbf{U}_{(n,m)})_{d+5,d+2} + (\mathbf{U}_{(n,m)})_{d+4,d+3}]$$

$$(\mathcal{Q}_{\mathbf{f}}^*(\mathbf{U}))_{(n,m)} = 2 [(\mathbf{U}_{(n,m)})_{d+4,d+2} + (\mathbf{U}_{(n,m)})_{d+5,d+3}]$$

for $(n,m) \in E$; and the adjoint with respect to \mathbf{v} is given by

$$(\mathcal{Q}_{\mathbf{v}}^*(\mathbf{U}))_n = \left[\sum_{(n,m) \in E} (\mathbf{U}_{(n,m)})_{d+2,d+2} + (\mathbf{U}_{(n,m)})_{d+3,d+3} \right]$$

$$+ \left[\sum_{(m,n) \in E} (U_{(m,n)})_{d+4,d+4} + (U_{(m,n)})_{d+5,d+5} \right].$$

for $n \in V$. ADMM for (12) has the following explicit form.

Theorem 1. *Let $\nu_n := |\{m \in V : (n, m) \in E\}| + |\{m \in V : (m, n) \in E\}|$ for $n \in V$. For $\rho > 0$, ADMM (11) applied to (12) reads as*

$$\begin{aligned} \mathbf{x}_n^{(k+1)} &:= \text{proj}_{\mathbb{A}_{d+1}} \left(\frac{1}{4\nu_n} (\mathcal{Q}_{\mathbf{x}}^*(\mathbf{U}^{(k)} - \mathbf{Z}^{(k)})_n + \frac{1}{\rho} \mathbf{y}_n) \right) \quad \forall n \in V, \\ \boldsymbol{\ell}^{(k+1)} &:= \frac{1}{4\rho} \mathcal{Q}_{\boldsymbol{\ell}}^*(\mathbf{U}^{(k)} - \mathbf{Z}^{(k)}), \\ \mathbf{f}^{(k+1)} &:= \frac{1}{4} (\mathcal{Q}_{\mathbf{f}}^*(\mathbf{U}^{(k)} - \mathbf{Z}^{(k)}) + \frac{\lambda}{\rho} \mathbf{1}_M) \\ \mathbf{v}_n^{(k+1)} &:= \frac{1}{2\nu_n} (\mathcal{Q}_{\mathbf{v}}^*(\mathbf{U}^{(k)} - \mathbf{Z}^{(k)})_n - \frac{1+\nu_n\lambda}{2\rho}) \quad \forall n \in V, \\ \mathbf{U}_{(n,m)}^{(k+1)} &:= \text{proj}_{\succeq \mathbf{0}} (\mathcal{Q}_{(n,m)}([\mathbf{x}, \boldsymbol{\ell}, \mathbf{f}, \mathbf{v}]^{(k+1)}) + \mathbf{E} + \mathbf{Z}_{(n,m)}^{(k)}) - \mathbf{E} \quad \forall (n, m) \in E, \\ \mathbf{Z}^{(k+1)} &:= \mathbf{Z}^{(k)} + \mathcal{Q}(\mathbf{U}^{(k+1)}) - \mathbf{U}^{(k+1)}, \end{aligned}$$

where $\text{proj}_{\mathbb{A}_{d+1}}$ is the projection onto \mathbb{A}_{d+1} , $\text{proj}_{\succeq \mathbf{0}}$ onto the positive semi-definite matrices, and $\mathbf{1}_{\bullet}$ is the all ones vector.

The projections can be computed explicitly, cf. [5, Thm. 5.2] and [8, p. 399]. For $\boldsymbol{\xi} \in \mathbb{R}^{d+1}$ and the eigenvalue decomposition $\mathbf{A} = \mathbf{V} \boldsymbol{\Sigma} \mathbf{V}^* \in \mathcal{S}_{d+5}$, we have

$$\text{proj}_{\mathbb{A}_{d+1}}(\boldsymbol{\xi}) = (\xi_1, \dots, \xi_d, \max\{\xi_{d+1}, 1\})^*, \quad (14a)$$

$$\text{proj}_{\succeq \mathbf{0}}(\mathbf{A}) = \mathbf{V} \max(\boldsymbol{\Sigma}, 0) \mathbf{V}^*. \quad (14b)$$

Proof. The minimizer of (11a) can be easily computed as in [5, Thm. 5.1]. The objective with \mathcal{F} chosen as $\mathcal{J} + \mathcal{I}$ is quadratic and decouples all variables. In order to compute the derivative, we can exploit

$$\begin{aligned} \mathcal{Q}_{\mathbf{x}}^*(\mathcal{Q}(\mathbf{x}, \boldsymbol{\ell}, \mathbf{f}, \mathbf{v}))_n &= 4\mathbf{x}_n, & \mathcal{Q}_{\boldsymbol{\ell}}^*(\mathcal{Q}(\mathbf{x}, \boldsymbol{\ell}, \mathbf{f}, \mathbf{v}))_{(n,m)} &= 4\boldsymbol{\ell}_{(n,m)}, \\ \mathcal{Q}_{\mathbf{f}}^*(\mathcal{Q}(\mathbf{x}, \boldsymbol{\ell}, \mathbf{f}, \mathbf{v}))_{(n,m)} &= 4\mathbf{f}_{(n,m)}, & \mathcal{Q}_{\mathbf{v}}^*(\mathcal{Q}(\mathbf{x}, \boldsymbol{\ell}, \mathbf{f}, \mathbf{v}))_n &= 2\mathbf{v}_n. \end{aligned}$$

For $(\mathbf{x}_n)_{d+1}$, we have the constraint $(\mathbf{x}_n)_{d+1} \geq 1$, which results in the projection onto \mathbb{A}_{d+1} . In (11b), $\mathbf{U}_{(n,m)}$ are decoupled, and we have

$$\begin{aligned} \mathbf{U}_{(n,m)}^{(k+1)} &= \arg \min_{\mathbf{U} \succeq -\mathbf{E}} \|\mathcal{Q}_{(n,m)}([\mathbf{x}, \boldsymbol{\ell}, \mathbf{f}, \mathbf{v}]^{(k+1)}) - \mathbf{U} + \mathbf{Z}_{(n,m)}^{(k)}\|_{\mathbb{F}}^2 \\ &= \left[\arg \min_{\tilde{\mathbf{U}} := \mathbf{U} + \mathbf{E} \succeq \mathbf{0}} \|(\mathcal{Q}_{(n,m)}([\mathbf{x}, \boldsymbol{\ell}, \mathbf{f}, \mathbf{v}]^{(k+1)}) + \mathbf{E} + \mathbf{Z}_{(n,m)}^{(k)}) - \tilde{\mathbf{U}}\|_{\mathbb{F}}^2 \right] - \mathbf{E} \\ &= \text{proj}_{\succeq \mathbf{0}}(\mathcal{Q}_{(n,m)}^{(k+1)} + \mathbf{Z}_{(n,m)}^{(k)}) - \mathbf{E}. \quad \square \end{aligned}$$

3.2 Solving the Relaxed TV denoising model

Similar to § 3.1, we rely on the following splitting, to solve (9):

$$\arg \min_{\mathbf{x}, \mathbf{v}, \mathbf{u}, \mathbf{U}} \mathcal{K}(\mathbf{x}, \mathbf{v}) + \mathcal{I}(\mathbf{u}) + \mathcal{H}(\mathbf{U}) \quad \text{s.t.} \quad \mathbf{x} = \mathbf{u} \quad \text{and} \quad \mathcal{V}(\mathbf{x}, \mathbf{v}) = \mathbf{U} \in \mathcal{S}_{d+3}^N. \quad (15)$$

Here, \mathcal{I} is defined as in (13) and

$$\mathcal{H}(\mathbf{U}) := \sum_{n \in V} \iota_{\hat{\mathcal{C}}}(\mathbf{U}_n),$$

where $\hat{\mathbf{E}} := \text{diag}(\mathbf{I}_{d+1}, \begin{bmatrix} 0 & -1 \\ -1 & 0 \end{bmatrix})$ and $\hat{\mathcal{C}} := \{\mathbf{A} \in \mathcal{S}_{d+3} : \mathbf{A} + \hat{\mathbf{E}} \succeq \mathbf{0}\}$. The linear operator $\mathcal{V} := (\mathcal{V}_n)_{n \in V}$ is defined as

$$\mathcal{V}_n(\mathbf{x}, \mathbf{v}) := \mathbf{V}_n - \hat{\mathbf{E}}.$$

To apply (11), we define $\|\mathbf{U}\|^2 := \sum_{n \in V} \|\mathbf{U}_n\|_{\mathbb{F}}^2$ and derive the adjoint of \mathcal{V} that—with respect to the arguments \mathbf{x} and \mathbf{v} —is given by

$$((\mathcal{V}_{\mathbf{x}}^*(\mathbf{U}))_n)_i = 2[(\mathbf{U}_n)_{i,d+2} + (-1)^{\delta_{i,d+1}}(\mathbf{U}_n)_{i,d+3}], \quad (16a)$$

$$(\mathcal{V}_{\mathbf{v}}^*(\mathbf{U}))_n = (\mathbf{U}_n)_{d+2,d+2} + (\mathbf{U}_n)_{d+3,d+3} \quad (16b)$$

for $n \in V$ and $1 \leq i \leq d+1$. ADMM for (15) has the following form.

Theorem 2. For $\rho > 0$, ADMM (11) applied to (15) reads as

$$\begin{aligned} \mathbf{x}^{(k+1)} &:= \text{prox}_{\mu/5\rho \text{ TV}}\left(\frac{1}{5}[\mathcal{V}_{\mathbf{x}}^*(\mathbf{U}^{(k)} - \mathbf{Z}^{(k)}) + \frac{1}{\rho} \mathbf{y} + (\mathbf{u}^{(k)} - \mathbf{z}^{(k)})]\right), \\ \mathbf{v}^{(k+1)} &:= \frac{1}{2\rho}(\rho \mathcal{V}_{\mathbf{v}}^*(\mathbf{U}^{(k)} - \mathbf{Z}^{(k)}) - \frac{1}{2} \mathbf{1}_N), \\ \mathbf{U}_n^{(k+1)} &:= \text{proj}_{\succeq \mathbf{0}}(\mathbf{V}_n^{(k+1)} + \mathbf{Z}_n^{(k)}) - \hat{\mathbf{E}} \quad \forall n \in V, \\ \mathbf{u}_n^{(k+1)} &:= \text{proj}_{\mathbb{A}_{d+1}}(\mathbf{x}_n^{(k+1)} + \mathbf{z}_n^{(k)}) \quad \forall n \in V, \\ \mathbf{Z}^{(k+1)} &:= \mathbf{Z}^{(k)} + \mathcal{V}([\mathbf{x}, \mathbf{v}]^{(k+1)}) - \mathbf{U}^{(k+1)}, \\ \mathbf{z}^{(k+1)} &:= \mathbf{z}^{(k)} + \mathbf{x}^{(k+1)} - \mathbf{u}^{(k+1)}, \end{aligned}$$

where $\text{prox}_f := \arg \min_{\mathbf{y}} \{f(\mathbf{y}) + \frac{1}{2} \|\cdot - \mathbf{y}\|^2\}$ for convex, lower semi-continuous, proper f .

The projection onto \mathbb{A}_{d+1} and the positive semi-definite matrices is known from (14). Further, we rely on an anisotropic TV regularization. Therefore, we can apply the fast TV programs [10, 11] coordinatewise to efficiently compute $\text{prox}_{\mu/4\rho \text{ TV}}$ for line and grid graphs, i.e. for signals and images, cf. [4, Rem. 4.1].

Proof. In the proof, we denote by $\llbracket \mathbf{A} \rrbracket_j$ the first $d+1$ entries of the j -th column of $\mathbf{A} \in \mathcal{S}_{d+3}$. Furthermore, let $\mathbf{e} := (1, \dots, 1, -1)^* \in \mathbb{R}^{d+1}$. Then, the adjoint in (16a) may be written as

$$(\mathcal{V}_{\mathbf{x}}^*(\mathbf{U}))_n = 2(\llbracket \mathbf{U}_n \rrbracket_{d+2} + \mathbf{e} \odot \llbracket \mathbf{U}_n \rrbracket_{d+3}) \quad \forall n \in V,$$

where \odot denotes the Hadamard product. In the first ADMM step (11a) for our splitting (15), the minimization with respect to \mathbf{x} and \mathbf{v} decouples. Using the symmetry of $\mathbf{U}^{(k)}$ and $\mathbf{Z}^{(k)}$, exploiting $\tilde{\mathbf{x}}_n = \mathbf{e} \odot \mathbf{x}_n$, and combining the squared norms and inner products, we can compute the minimizer with respect to \mathbf{x} by

$$\arg \min_{\mathbf{x} \in (\mathbb{R}^{d+1})^N} \left\{ \frac{1}{2} \sum_{n \in V} (v_n - 2\langle \mathbf{x}_n, \mathbf{y}_n \rangle) + \mu \text{TV}(\mathbf{x}) + \frac{\rho}{2} \sum_{n \in V} \|\mathbf{x}_n - \mathbf{u}_n^{(k)} + \mathbf{z}_n^{(k)}\|_2^2 \right\}$$

$$\begin{aligned}
& + \frac{\rho}{2} \sum_{n \in V} \|\mathcal{V}_n(\mathbf{x}, \mathbf{v}) - \mathbf{U}_n^{(k)} + \mathbf{Z}_n^{(k)}\|_F^2 \Big\} \\
& = \arg \min_{\mathbf{x} \in (\mathbb{R}^{d+1})^N} \left\{ - \sum_{n \in V} \langle \mathbf{x}_n, \mathbf{y}_n \rangle + \mu \text{TV}(\mathbf{x}) + \rho \sum_{n \in V} \left[\frac{1}{2} \|\mathbf{x}_n - \mathbf{u}_n^{(k)} + \mathbf{z}_n^{(k)}\|_2^2 \right. \right. \\
& \quad \left. \left. + \|\mathbf{x}_n - \llbracket \mathbf{U}_n^{(k)} \rrbracket_{d+2} + \llbracket \mathbf{Z}_n^{(k)} \rrbracket_{d+2}\|_2^2 + \|\tilde{\mathbf{x}}_n - \llbracket \mathbf{U}_n^{(k)} \rrbracket_{d+3} + \llbracket \mathbf{Z}_n^{(k)} \rrbracket_{d+3}\|_2^2 \right] \right\} \\
& = \arg \min_{\mathbf{x} \in (\mathbb{R}^{d+1})^N} \left\{ - \sum_{n \in V} \langle \mathbf{x}_n, \mathbf{y}_n \rangle + \mu \text{TV}(\mathbf{x}) \right. \\
& \quad \left. + \frac{5\rho}{2} \sum_{n \in V} \|\mathbf{x}_n - \frac{1}{5} [\mathcal{V}_{\mathbf{x}}^*(\mathbf{U} - \mathbf{Z})_n + (\mathbf{u}^{(k)} - \mathbf{z}^{(k)})_n]\|_2^2 \right\} \\
& = \arg \min_{\mathbf{x} \in (\mathbb{R}^{d+1})^N} \left\{ \frac{5\rho}{2} \sum_{n \in V} \|\mathbf{x}_n - \frac{1}{5} [\mathcal{V}_{\mathbf{x}}^*(\mathbf{U} - \mathbf{Z})_n + \frac{\mathbf{y}_n}{\rho} + (\mathbf{u}_n - \mathbf{z}_n)]\|_2^2 + \mu \text{TV}(\mathbf{x}) \right\},
\end{aligned}$$

Because of the differentiability of the objective with respect to \mathbf{v} , and since $\mathcal{V}_{\mathbf{v}}^*(\mathcal{V}(\mathbf{x}, \mathbf{v})) = 2\mathbf{v}$, the minimizer is given by

$$\begin{aligned}
\mathbf{0}_N &= \frac{1}{2} \mathbf{1}_N + \rho \mathcal{V}_{\mathbf{v}}^*(\mathcal{V}_{\mathbf{v}}(\mathbf{x}, \mathbf{v}) - \mathbf{U}^{(k)} + \mathbf{Z}^{(k)}), \quad \text{and thus} \\
\mathbf{v}^{(k+1)} &= \frac{1}{2} [\mathcal{V}_{\mathbf{v}}^*(\mathbf{U}^{(k)} - \mathbf{Z}^{(k)}) - \frac{1}{2\rho} \mathbf{1}_N].
\end{aligned}$$

The two subproblems with respect to \mathbf{U} and \mathbf{u} of the second ADMM step (11b) regarding (15) can be treated similarly to the proof of Thm. 1 yielding the projection onto the positive semi-definite matrices and \mathbb{A}_{d+1} . \square

4 Numerical Experiments

The derived algorithms in Thm. 1 and 2 are implemented¹ in Python 3.11.4 using Numpy 1.25.0 and Scipy 1.11.1. The experiments are performed on an off-the-shelf iMac 2020 with Apple M1 Chip (8-Core CPU, 3.2 GHz) and 8 GB RAM. The convergence of both algorithms is ensured by [3, Cor. 28.3]. For all experiments, the methods are initialized by zeros for all variables. The resulting implementations are very similar to the ones proposed for sphere- and SO(3)-valued data in [4, 5].

Synthetic Image Processing. In this subsection, we give a proof of the concept for both models—the Tikhonov-like and TV model—based on synthetic data. For the ground truth \mathbf{x}_{true} of the two experiments, see Fig. 1, we interpolate points in \mathbb{R} or \mathbb{R}^2 and apply the smooth mappings

$$\mathbf{x}_{\mathbb{H}_1} : \mathbb{R} \rightarrow \mathbb{H}_1, \quad r \mapsto (\sinh(r), \cosh(r))^*, \quad (17a)$$

$$\mathbf{x}_{\mathbb{H}_2} : \mathbb{R}^2 \rightarrow \mathbb{H}_2, \quad (r, s) \mapsto (\sinh(r) \cos(s), \sinh(r) \sin(s), \cosh(r))^*. \quad (17b)$$

In the first experiment, where an one-dimensional signal of length 400, i.e. a signal on a line graph, is considered, the noisy measurements $\mathbf{y} \in \mathbb{H}_1^{400}$ are

¹ The code is available at GitHub: https://github.com/JJEWBresch/relaxed_tikhonov_regularization.

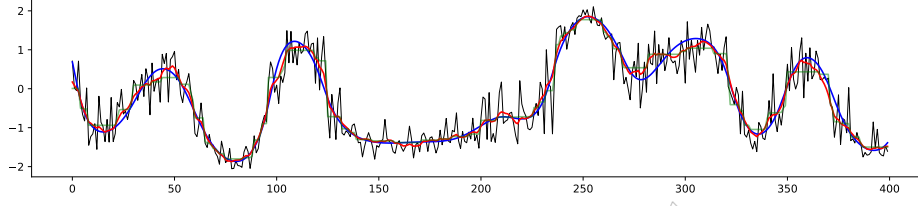
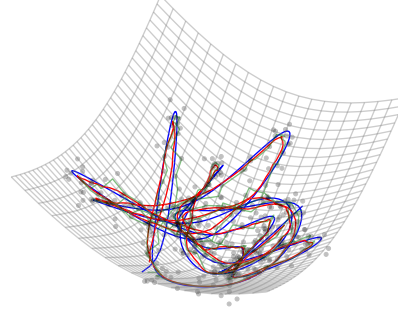


Fig. 1. Restoration of smooth synthetic line signals (blue) from noisy measurements (black/gray). For the Tikhonov model (red), we choose $\rho = 10^{-1}$, $\lambda = 6$ (top) and $\lambda = 5$ (right). For the TV model (green), we choose $\rho = 1$, $\mu = 0.75$ (top), and $\mu = 0.1$ (right). Note that the \mathbb{H}_1 signal (top) is visualized using the parametrization in (17a). The \mathbb{H}_2 signal (right) is directly visualized on the hyperbolic sheet in $\mathbb{A}_3 \subset \mathbb{R}^3$.



generated employing the tangential normal distribution [19] with standard deviation $\sigma := 0.6$, see Fig. 1 (top). The \mathbb{H}_1 -valued signals are here illustrated via the parameter r in (17a). Applying ADMM from Thm. 1 and 2 for the Tikhonov-like and TV model respectively, we observe convergence to the hyperbolic sheet. In both cases, the mean absolute error (MAE) with respect to the Minkowski bilinearform $\eta \equiv -1$ is 10^{-4} at the most. The restored signals after 12 sec. and the used parameters are recorded in Fig. 1 (top).

In the second experiment, we consider a line signal of length 400 with values in \mathbb{H}_2 . The noisy measurements are generated via additive Gaussian noise, i.e. $\mathbf{y} \sim \mathcal{N}(\mathbf{x}_{\text{true}}, \sigma^2 \mathbf{I})$ with $\sigma := 0.3$. Note that the measurements lie in \mathbb{R}^3 and not necessarily on \mathbb{H}_2 . The denoised signals using ADMM for both models are shown in Fig. 1 (right). After 80 sec., we recorded an MAE with respect to $\eta \equiv -1$ of 10^{-5} at the most. Because of convergence back to the hyperbolic sheet, the numerical solutions are actual solutions of the non-convex model (1) and (6) respectively.

Gaussian Image Processing. The idea behind Gaussian image processing is that, instead of a single image, we measure a series of K noisy instances, where we assume that each pixel $x_{i,j}^{(k)}$ follows a Gaussian distribution. The empirical mean and variance may be estimated by the maximum likelihood estimators

$$\hat{\mu}_{ij} := \frac{1}{K} \sum_{k=1}^K x_{i,j}^{(k)}, \quad \hat{\sigma}_{ij}^2 := \frac{1}{K} \sum_{k=1}^K (x_{i,j}^{(k)} - \hat{\mu}_{ij})^2. \quad (18)$$

The set of Gaussians $\mathcal{N}(\mu, \sigma)$ parameterized by $(\mu, \sigma) \in \mathbb{R} \times \mathbb{R}_{>0}$ and equipped with the so-called Fisher metric is isometric to the hyperbolic space \mathbb{H}_2 . More

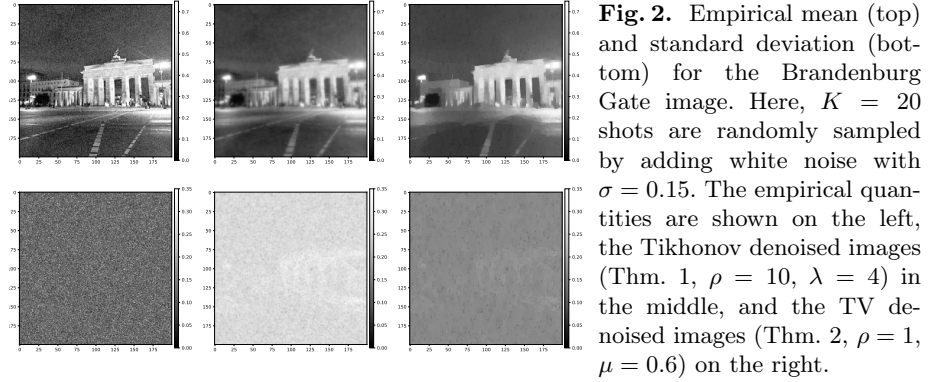


Fig. 2. Empirical mean (top) and standard deviation (bottom) for the Brandenburg Gate image. Here, $K = 20$ shots are randomly sampled by adding white noise with $\sigma = 0.15$. The empirical quantities are shown on the left, the Tikhonov denoised images (Thm. 1, $\rho = 10$, $\lambda = 4$) in the middle, and the TV denoised images (Thm. 2, $\rho = 1$, $\mu = 0.6$) on the right.

precisely, the isometry is given by $\pi_3 \circ \pi_2 \circ \pi_1: \mathcal{N} \rightarrow \mathbb{H}_2$ with

$$\pi_1: \mathcal{N} \rightarrow \mathbb{P}_2, \quad (\mu, \sigma) \mapsto \frac{1}{\sqrt{2}}(\mu, \sqrt{2}\sigma)^*, \quad (19a)$$

$$\pi_2: \mathbb{P}_2 \rightarrow \mathbb{D}_2, \quad \mathbf{y} \mapsto \frac{1}{y_1^2 + (y_2 + 1)^2} (2y_1, \|\mathbf{y}\|_2^2 - 1)^*, \quad (19b)$$

$$\pi_3: \mathbb{D}_2 \rightarrow \mathbb{H}_2, \quad \mathbf{y} \mapsto \frac{1}{1 - \|\mathbf{y}\|_2^2} (2y_1, 2y_2, 1 + \|\mathbf{y}\|_2^2)^*, \quad (19c)$$

where $\mathbb{D}_2 := \{\mathbf{x} \in \mathbb{R}^2 : \|\mathbf{x}\|_2 < 1\}$ is the Pioncaré disc, and the Pioncaré half-space is given by $\mathbb{P}_2 := \{\mathbf{x} \in \mathbb{R}^2 : x_2 > 0\}$, see [6, 20].

In the first experiment, as proof of concept, we consider a gray-valued image of the Brandenburg Gate and generate a series of 20 images by adding Gaussian white noise with constant standard deviation. Calculating the empirical mean and variance pixelwise, and using the isometry in (19), we obtain an \mathbb{H}_2 -valued image. Afterwards we denoise mean and variance simultaneously using the algorithms from Thm. 1 and 2. The results are recorded in Fig. 2. Analyzing the qualitative outcomes, we conclude that both models are adequate ansätze. The Tikhonov-like model, however, overestimates the standard deviation.

In the second experiment, we consider a real-world application of Gaussian image processing, where 20 highly noisy images of a retina are given. The experiment originates from [1], and the goal is again to denoise mean and variance simultaneously. The qualitative results of the Tikhonov-like and TV denoising are shown in Fig. 3. The Tikhonov-like model again overestimates the standard deviation. During the denoising, we observe numerical convergence to the hyperbolic sheet. More precisely, we reach an MAE of at most 10^{-4} with respect to $\eta \equiv -1$ in 15 min. for the Tikhonov-like model and in 3 min. for the TV model. The numerical solutions are thus solutions of the non-convex models (1) and (6), too. For the TV proximity mapping in Thm. 2, we use the TV program (ADRA) [10] with $\gamma = 1$ as subprocedure. A quantitative comparison with the Proximal Douglas–Rachford Algorithm (PDRA) [6] for more generally manifold-valued data is given in Tab. 1. Our relaxed Euclidean models here yield comparable results with respect to the SNR (signal-to-noise ratio) and the computation time.

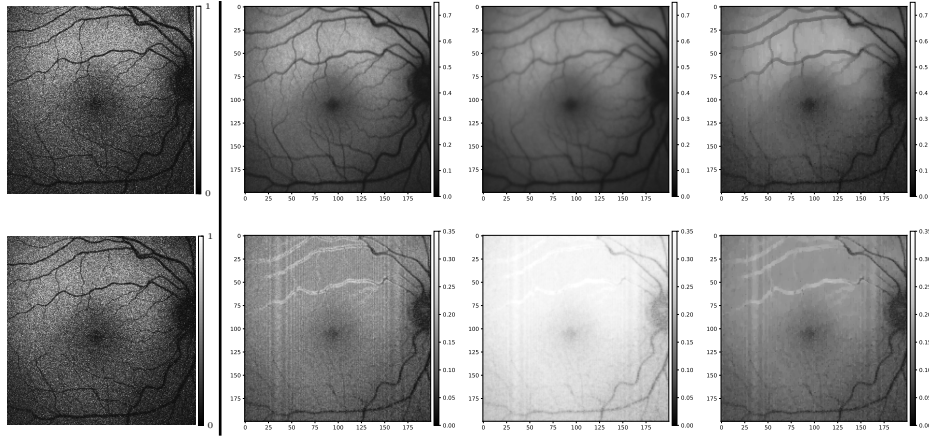


Fig. 3. Clearing the estimated mean and standard deviation of $K = 20$ retina scans. *Leftmost:* the 1st (top) and 20th (bottom) image of the retina scans. *From left to right:* the empirical mean (top) and standard deviation (bottom); Tikhonov denoised images (Thm. 1, $\lambda = 1.5$, $\rho = 10$); TV denoised images (Thm. 2, $\mu = 0.15$, $\rho = 1$).

ADMM from Thm. 2 ($\rho = 1$)						PDRA ($\eta = 0.5, \lambda = 0.9$)			
SNR($\hat{\mu}$)	SNR($\hat{\sigma}$)	μ	\mathcal{K}	MEA $\eta \equiv -1$	time (sec.)	SNR($\hat{\mu}$)	SNR($\hat{\sigma}$)	α	time (sec.)
6.121	12.211	0.05	$2.61 \cdot 10^5$	$4.73 \cdot 10^{-4}$	160	5.963	12.400	0.1	120
6.001	12.369	0.10	$2.54 \cdot 10^5$	$4.78 \cdot 10^{-4}$	180	5.911	12.618	0.3	140
5.986	12.301	0.15	$1.81 \cdot 10^5$	$4.47 \cdot 10^{-4}$	190	5.874	12.748	0.5	280
5.966	12.455	0.20	$1.19 \cdot 10^5$	$4.67 \cdot 10^{-4}$	220	5.843	12.849	0.7	430

Table 1. Comparison of the TV denoising (Thm. 2) and PDRA (Douglas–Rachford) [6] regarding the SNR for the restored mean and standard deviation. The marked instance ($\mu = 0.15$) is visualized in Fig. 3.

Acknowledgements We would like to thank R. Bergmann, J. Persch and G. Steidl for providing the data of the retina experiment, and G. Steidl for drawing the attention to this experiments. Originally, the data was provided by J. Angulo.

References

1. Angulo, J., Velasco-Forero, S.: Morphological processing of univariate Gaussian distribution-valued images based on Poincaré upper-half plane representation, pp. 331–366. Springer, Cham (2014). https://doi.org/10.1007/978-3-319-05317-2_12
2. Atigh, M.G., Schoep, J., Acar, E., Van Noord, N., Mettes, P.: Hyperbolic image segmentation. In: Proceedings of the CVPR ’22. pp. 4443–4452 (2022). <https://doi.org/10.1109/CVPR52688.2022.00441>
3. Bauschke, H.H., Combettes, P.L.: Convex Analysis and Monotone Operator Theory in Hilbert Spaces. Springer, New York (2011). <https://doi.org/10.1007/978-1-4419-9467-7>
4. Beinert, R., Bresch, J.: Denoising sphere-valued data by relaxed total variation regularization (2024), <https://arxiv.org/abs/2404.13181>
5. Beinert, R., Bresch, J., Steidl, G.: Denoising of sphere- and $SO(3)$ -valued data by relaxed Tikhonov regularization. Inverse Probl. Imaging (2024). <https://doi.org/10.3934/ipi.2024026>

6. Bergmann, R., Persch, J., Steidl, G.: A parallel Douglas-Rachford algorithm for minimizing ROF-like functionals on images with values in symmetric Hadamard manifolds. *SIAM J. Imaging Sci.* **9**(3), 901–937 (2016). <https://doi.org/10.1137/15M1052858>
7. Boguñá, M., Papadopoulos, F., Krioukov, D.: Sustaining the internet with hyperbolic mapping. *Nat. Commun.* **1**(1), 62 (2010). <https://doi.org/10.1038/ncomms1063>
8. Boyd, S., Vandenberghe, L.: *Convex Optimization*. Cambridge University Press, Cambridge (2004). <https://doi.org/10.1017/CBO9780511804441>
9. Chossat, P., Faugeras, O.: Hyperbolic planforms in relation to visual edges and textures perception. *PLoS Comput. Biol.* **5**(12), 1–16 (2009). <https://doi.org/10.1371/journal.pcbi.1000625>
10. Condat, L.: A direct algorithm for 1D total variation denoising (2012), <https://hal.science/hal-00675043>
11. Condat, L.: A direct algorithm for 1D total variation denoising. *IEEE Signal Process. Lett.* **20**(11), 1054–1057 (2013). <https://doi.org/10.1109/LSP.2013.2278339>
12. Condat, L.: Tikhonov regularization of circle-valued signals. *IEEE Trans. Signal Process.* **70**, 2775–2782 (2022). <https://doi.org/10.1109/TSP.2022.3179816>
13. Ganea, O.E., Bécigneul, G., Hofmann, T.: Hyperbolic neural networks. In: *Adv. Neural Inf. Process. Syst.* pp. 5350–5360. Curran Associates, New York (2018), https://proceedings.neurips.cc/paper_files/paper/2018/file/dbab2adc8f9d078009ee3fa810bea142-Paper.pdf
14. Glowinski, R., Marroco, A.: Sur l’approximation, par éléments finis d’ordre un, et la résolution, par pénalisation-dualité d’une classe de problèmes de dirichlet non linéaires. *R.A.I.R.O. Analyse Numérique* **9**(R2), 41–76 (1975). <https://doi.org/10.1051/m2an/197509R200411>
15. Hopf, H.: Zum Clifford-Kleinschen Raumproblem. *Math. Ann.* **95**, 313–339 (1926)
16. Horn, R.A., Johnson, C.R.: *Matrix Analysis*. Cambridge University Press, Cambridge, 2nd edn. (2012). <https://doi.org/10.1017/CBO9780511810817>
17. Killing, W.: Ueber die Clifford-Klein’schen Raumformen. *Math. Ann.* **39**, 257–278 (1891)
18. Krioukov, D., Papadopoulos, F., Kitsak, M., Vahdat, A., Boguñá, M.: Hyperbolic geometry of complex networks. *Phys. Rev. E* **82**, 036106 (2010). <https://doi.org/10.1103/PhysRevE.82.036106>
19. Laus, F.J.: *Statistical Analysis and Optimal Transport for Euclidean and Manifold-Valued Data*. Dr. Hut, München (2020)
20. Lee, J.: *Riemannian Manifolds: An Introduction to Curvature*. Springer, New York (1997). <https://doi.org/10.1007/b98852>
21. Lin, F., Bai, B., Guo, Y., Chen, H., Ren, Y., Xu, Z.: MHCN: A hyperbolic neural network model for multi-view hierarchical clustering. In: *Proceedings of the ICCV ’23*. pp. 16479–16489 (2023). <https://doi.org/10.1109/ICCV51070.2023.01515>
22. Liu, Q., Nickel, M., Kiela, D.: Hyperbolic graph neural networks. In: *Adv. Neural Inf. Process. Syst.* vol. 32. Curran Associates (2019), https://proceedings.neurips.cc/paper_files/paper/2019/file/103303dd56a731e377d01f6a37badae3-Paper.pdf
23. Nickel, M., Kiela, D.: Poincaré embeddings for learning hierarchical representations. In: *Adv. Neural Inf. Process. Syst.* vol. 30. Curran Associates (2017), https://proceedings.neurips.cc/paper_files/paper/2017/file/59dfa2df42d9e3d41f5b02bfc32229dd-Paper.pdf
24. Wald, R.M.: *General Relativity*. Chicago University Press, Chicago (1984). <https://doi.org/10.7208/chicago/9780226870373.001.0001>